A Probabilistic Load Margin Assessment Method for Active Distribution Networks

Liu Yunxin, Yao Liangzhong, Liao Siyang, Deng Jinglei
School of Electrical Engineering and Automation
Wuhan University
Wuhan, China

Sheng Wangxing, Liu Keyan
China Electric Power Research Institute
Beijing, China

***Abstract*—With the high-penetration integration of distributed energy resources (DERs), such as distributed photovoltaics (PVs) and plug-in electric vehicles (PEVs), into distribution networks, their inherent characteristics, including strong stochasticity and dynamic characteristics, pose significant challenges to static voltage stability. To address this issue, this paper proposes a probabilistic static voltage stability assessment method for active distribution networks First, the probabilistic power characteristics of DERs are modeled, and the operational constraints imposed by low-voltage ride-through (LVRT) requirements and inverter current limitations are analyzed. Then, an improved continuation power flow (CPF), in which we propose a new predictor-corrector considering dynamic characteristics, is developed to accurately quantify their impact on load margin. Finally, Monte Carlo simulation combined with kernel density estimation (KDE) is employed to construct the probability distribution of load margin. The effectiveness of the proposed method are validated on a modified IEEE 33-bus and IEEE 141-bus distribution system.**

Keywords—high-penetration distributed energy resources; active distribution networks; load margin; improved continuation power flow; probabilistic assessment.

I. INTRODUCTION

Distributed energy resources are integrated into distribution systems via converters that incorporate current limitations in their control loops. When the voltage at the point-of-common-coupling (U_{PCC}) drops, the active and reactive power regulation capability of these resources is significantly reduced. Moreover, DERs are prone to unintentional disconnection under low-voltage conditions, which can trigger cascading tripping events and further deteriorate the static voltage stability of the distribution system [1]-[2].

Most studies address the impact of current limitations and low-voltage tripping behavior on short-term voltage stability and fault-ride-through requirements [3]-[4]. One study [5]focused on current limitations for voltage-controlled inverters during overloads caused by poor transient load sharing between inverters and synchronous generators in islanded microgrids. Another study [6] has shown that significant disturbances leading to PV inverter trips or slow LVRT responses can severely affect ST voltage stability. Moreover, the impact of the abrupt loss of PV systems on dynamic voltage stability under various bus voltage conditions has been investigated [7]. To the best of the authors' knowledge, the literature still lacks a wider and more detailed analysis considering the effects of current limitations and low-voltage tripping behavior on static voltage stability with a detailed representation of system dynamics.

Significant progress has been made in the probabilistic assessment of static voltage stability, as evidenced by extensive domestic and international research [8-14]. Commonly used approaches include Monte Carlo simulation [8-9], the cumulant-based method [10], and point estimation [11]. In a previous study [12], the Nataf transformation combined with Monte Carlo simulation was employed for the probabilistic evaluation of static voltage stability margins. Additionally, Cholesky decomposition was integrated with stochastic response surface methods, and nonlinear programming was applied to compute the voltage stability margins [13]. Notably, intervariable correlations were considered in the probabilistic assessment framework [14]. However, these existing works often lack sufficient modeling granularity for the stochastic behavior of large-scale DERs and do not adequately address scenario generation under high DER penetration.

This paper proposes a probabilistic assessment method for static voltage stability margins in active distribution networks with high-penetration DERs, explicitly accounting for dual-side uncertainties from both generation and flexible loads. The strong stochasticity of both PV generation and EV charging loads is characterized, and individual forecasting errors of PV and load are accurately modeled using the generalized error distribution (GED) and the generalized lambda distribution (GLD). And the dynamic characteristics of DERs is analyzed by modeling the effects of current limitations and low-voltage tripping behavior on static voltage stability. On the basis of this, an improved CPF is developed that incorporates dynamic characteristics of DERs. Finally, A Monte Carlo–based probabilistic assessment framework is established to obtain the full probability distribution of load margin. Two complementary metrics, the expected load margin and the load margin risk index, are introduced. The effectiveness and accuracy of the proposed method are validated on modified IEEE 33-bus and IEEE 141-bus distribution networks. Compared with existing probabilistic voltage stability studies that model DERs as ideal PQ sources, the proposed method adopts a new predictor-corrector considering dynamic characteristics, so that it can yield more accurate load margin.

II. DYNAMIC CHARACTERISTICS OF DERS

If the current is too high, damage may occur to the semiconductors in the DER. So, current limitation is necessary. To provide both active and reactive power support, this paper uses the dq-axis axis current proportional limit. The dq-axis output current is as follows:

$$I_d^* = \begin{cases} I_d^{**} & I_d \leqslant I_{d\max} = k_{dq} I_{\max} \\ I_{d\max} & I_d > I_{d\max} = k_{dq} I_{\max} \end{cases} \tag{1}$$

XXX-X-XXXX-XXXX-X/XX/$XX.00 ©20XX IEEE
979-8-3315-8138-1

$$I_q^* = \begin{cases} I_q^{**} & I_q \leqslant I_{q\max} = \sqrt{1-k_{dq}^2} I_{\max} \\ I_{q\max} & I_q > I_{q\max} = \sqrt{1-k_{dq}^2} I_{\max} \end{cases} \quad (2)$$

where $I_{\max}$ is the inverter current limitation value, I_d^{**} is the d-axis current command, I_q^{**} is the q-axis current command and k_{dq} is the proportional value.

DERs exhibit limited tolerance to voltage fluctuations. The grid code in China typically specifies the allowable voltage operating range for DERs and the conditions under which disconnection is permitted [15] (Fig. 1).

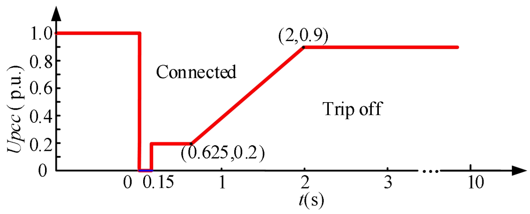

Fig. 1. LVRT time of national grid code in China.

The topology of a single-machine infinite-bus system with integrated distributed generation is shown in Fig. 2, and the corresponding simulation model is implemented in PSCAD. DG units are connected to the grid using the PQ control strategy. The simulated P-V and Q-V characteristics of the DERs under a continuously increasing load are shown in Fig. 3, capturing the effects of current limitations and low-voltage tripping behavior.

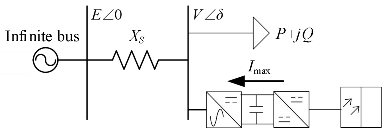

Fig. 2. Diagram of a single DER grid-connected system.

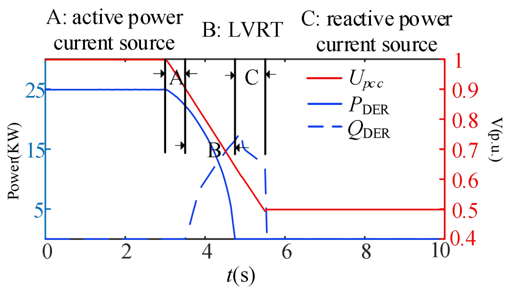

Fig. 3. Power characteristic curve of a DER.

As shown in Fig. 3, when $U_{\rm pcc}$ decreases, DERs initially increase their active current output to maintain constant active power. Once the current limit is reached, the active power output begins to decrease proportionally with the voltage, exhibiting constant-current-source-like behavior, corresponding to segment A. When the $U_{\rm PCC}$ falls below 0.9 p.u., the DERs inject reactive power in accordance with the grid code and mandated by the LVRT requirements, as illustrated in segment B. However, under continuously increasing load demand, the $U_{\rm PCC}$ continues to decline. Consequently, once the maximum reactive current capability is reached, the reactive power output also starts to decrease with further voltage reduction, again manifesting constant-current-source characteristics—as depicted in segment C. If $U_{\rm PCC}$ remains below 0.9 p.u. for more than 2 seconds, DERs will disconnect because of undervoltage protection.

III. Stochastic Modeling of DERs

A. Distributed PV and load Forecasting Error Model

In this paper, GED is used to fit the PV forecasting error, and its distribution function is as follows:

$$f\left(\Delta P_{PV}\right) = \frac{a}{b \cdot \Gamma(1/a)} \cdot \exp\left[-\frac{1}{2}\left|\frac{\Delta P_{PV} - c}{b}\right|^a\right] \quad (3)$$

$$b = \left[\frac{2^{2-\frac{2}{a}} \cdot \Gamma\left(\frac{1}{a}\right)}{\Gamma\left(\frac{3}{a}\right)}\right]^{\frac{1}{2}} \quad (4)$$

where a and b are shape parameters, c is the location parameter, and $\Gamma(\cdot)$ denotes the gamma function, $\Delta P_{\rm PV}$ is power forecasting deviation of the distributed PV. In this study, the GLD is employed to model load uncertainty, and its distribution function is given as follows:

$$f(\Delta P_{Load}) = \frac{AB\mathrm{e}^{-A(\Delta P_{Load} - C)}}{\left(1 + \mathrm{e}^{-A(\Delta P_{Load} - C)}\right)^{B+1}} \quad (5)$$

where A, B, and C are the fitting parameters of the GLD, $\Delta P_{\rm Load}$ is power forecasting deviation of the load.

B. PEV Forecasting Model

The initial charging time of a PEV follows a normal distribution [16-17]:

$$f_s(t) = \frac{1}{\sigma_s\sqrt{2\pi}} \exp[-\frac{(t-\mu_s)^2}{2\sigma_s}] \quad (6)$$

where t denotes the initial charging start time of the PEV and μ_s and δ_s represent the mean and standard deviation, respectively, reflecting statistical variations in user travel behavior.

The daily driving distance of PEVs follows the probability distribution proposed in the literature [16-17]:

$$f_D(t) = \frac{1}{D\sigma_D\sqrt{2\pi}} \exp[-\frac{(\ln D - \mu_D)^2}{2\sigma_D^2}] \quad (7)$$

where D denotes the daily driving mileage, and μ_D and δ_D represent the mean and standard deviation of ln D, respectively.

IV. Probabilistic Load Margin Assessment Method

A. Improved Continuation Power Flow

The parameterized power flow equation in the CPF [18] model is as follows:

$$f(\mathbf{V}, \boldsymbol{\theta}) + \lambda \mathbf{b} = 0 \quad (8)$$

where $\boldsymbol{b}$ is the vector of the generator and the load power change mode, including the direction and magnitude. λ represents the load parameter. The load margin is defined as:

$$K_{\rm p} = \frac{P_{\max} - P_0}{P_{\max}} \times 100\% \quad (9)$$

where P_0 is the load active power at the current operating point, $P_{\max}$ is the maximum load active power. By continually increasing the loading level, CPF involves multiple predictive and corrective directions to obtain the load margin. However, traditional CPF models DERs as ideal PQ sources, which can not reflect the dynamic characteristic. Accordingly, this paper proposes an improved CPF that considers the DER current limitation and low-voltage tripping behavior. The flow is shown in Fig. 4. The specific steps are as follows:

1) Before CPF calculation, calculate $I_{d\max}$ and $I_{q\max}$ of each DER. If $P_{\mathrm{DER}i}$ exceeds $P_{\mathrm{DER}i\max}$ or $Q_{\mathrm{DER}i}$ exceeds $Q_{\mathrm{DER}i\max}$ after the end of the nth correction, PCC is converted to the P-I_q node, I_d-Q node or I_d-I_q node.

2) Based on the voltage $U'_i(n)$, $I_{d\max}$ and $I_{q\max}$, the $P'_{\mathrm{DER}i}$ and $Q'_{\mathrm{DER}i}$ can be obtained.

3) $P'_{\mathrm{DER}i}$ and $Q'_{\mathrm{DER}i}$ are taken into the n+1 correction, when convergence is achieved. $P'_{\mathrm{DER}i}$ and $Q'_{\mathrm{DER}i}$ considering current limitation could also be obtained. In (10), λ is the control variables, other variables are state variables.

$$\begin{bmatrix} \boldsymbol{P}' \\ U_i'(n)I_{d\max i}^{DER} \ \ or \\ U_i'(n)I_{q\max i}^{DER} \\ \boldsymbol{Q}' \end{bmatrix} \begin{bmatrix} \left.\dfrac{\partial \boldsymbol{P}}{\partial \boldsymbol{\delta}}\right|_{n+1} & \left.\dfrac{\partial \boldsymbol{P}}{\partial \lambda}\right|_{n+1} & \left.\dfrac{\partial \boldsymbol{P}}{\partial \boldsymbol{U}}\right|_{n+1} \\ \left.\dfrac{\partial \boldsymbol{Q}}{\partial \boldsymbol{\delta}}\right|_{n+1} & \left.\dfrac{\partial \boldsymbol{Q}}{\partial \lambda}\right|_{n+1} & \left.\dfrac{\partial \boldsymbol{Q}}{\partial \boldsymbol{U}}\right|_{n+1} \end{bmatrix} = \begin{bmatrix} \Delta\boldsymbol{\delta} \\ \Delta\lambda \\ \Delta\boldsymbol{U} \end{bmatrix} \tag{10}$$

4) If the power output of other nodes is limited, take the same measures to iteratively solve the actual power output.

5) If $U_{\mathrm{PCC}i}$ falls below 0.9 p.u during the $(n+1)^{\mathrm{th}}$ correction, it is reclassified as an P-I_{q} node. And if, in the $(n+2)^{\mathrm{th}}$ correction, the $U_{\mathrm{PCC}i}$ remains below 0.9 p.u., the i^{th} DER will be disconnected.

$$\begin{bmatrix} \boldsymbol{P}' \\ 0 \\ 0 \\ \boldsymbol{Q}' \end{bmatrix} \begin{bmatrix} \left.\dfrac{\partial \boldsymbol{P}}{\partial \boldsymbol{\delta}}\right|_{n+2} & \left.\dfrac{\partial \boldsymbol{P}}{\partial \lambda}\right|_{n+2} & \left.\dfrac{\partial \boldsymbol{P}}{\partial \boldsymbol{U}}\right|_{n+2} \\ \left.\dfrac{\partial \boldsymbol{Q}}{\partial \boldsymbol{\delta}}\right|_{n+2} & \left.\dfrac{\partial \boldsymbol{Q}}{\partial \lambda}\right|_{n+2} & \left.\dfrac{\partial \boldsymbol{Q}}{\partial \boldsymbol{U}}\right|_{n+2} \end{bmatrix} = \begin{bmatrix} \Delta\boldsymbol{\delta} \\ \Delta\lambda \\ \Delta\boldsymbol{U} \end{bmatrix} \tag{11}$$

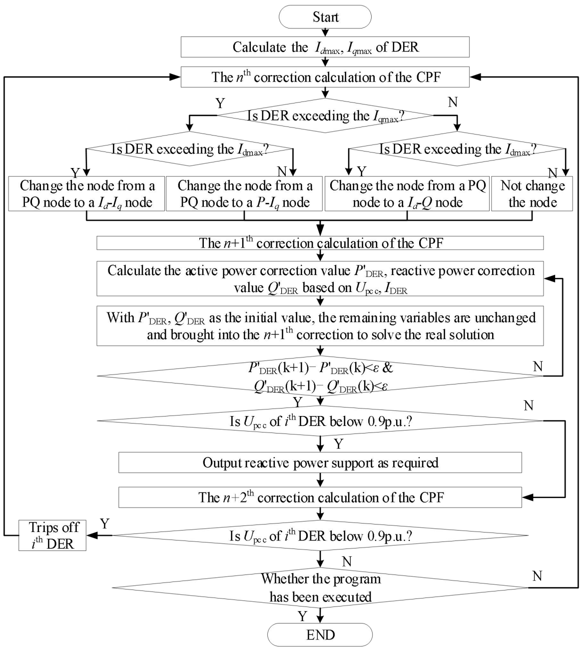

Fig. 4. Improved CPF considering DER dynamic characteristics.

B. Probabilistic Static Voltage Stability Indicator

In this paper, kernel density estimation (KDE) is employed to smoothly fit the ensemble of load margin across multiple scenarios, thereby deriving underlying probability distribution. The KDE kernel function is as follows [19]:

$$\hat{f}_h(x) = \frac{1}{nh}\sum_{i=1}^{n} K\left(\frac{x - x_i}{h}\right) \tag{12}$$

where h represents the bandwidth; x_i denotes the sample points of load margin; and $K(.)$ is the kernel function. This paper employs a Gaussian kernel function, as shown in (12):

$$K(v) = \frac{1}{\sqrt{2\pi}}\exp\left(-\frac{1}{2}v^2\right) \tag{13}$$

On the basis of the obtained probability distribution, this paper employs two complementary metrics, the expected load margin and the load margin risk index, to comprehensively characterize the static voltage stability of power systems with high penetration of DERs.

(1) Expected Load Margin S :

$$S = \int_{-\infty}^{+\infty} K_{\mathrm{P}}\hat{f}_h(K_{\mathrm{P}})dK_{\mathrm{P}} \tag{14}$$

where $\hat{f}_h(K_{\mathrm{P}})$ is probability distribution function.

(2) Load Margin Risk Index R

$$R = \int_{-\infty}^{\sigma} \hat{f}_h(K_{\mathrm{P}})dK_{\mathrm{P}} \tag{15}$$

where σ represents the critical threshold of load margin. In China, σ is 0.15-0.2 [21], and in North American, σ is 0.2 [22]. In this paper, σ is 0.2.

V. Simulation and Analysis

The effectiveness of the proposed method is validated in modified IEEE 33-bus and IEEE 141-bus distribution network, the detailed parameters of which are provided in MATPOWER 4.1 [23]. Since this paper primarily focuses on static voltage stability, the typical load level is set to 2.5 times the system base load to simulate a heavy loading condition. In IEEE 33-bus system, the base-case load demand is 9.29 + j5.75 MVA, and in IEEE 141-bus system, the base-case load demand is 29.86 + j18.51 MVA. The peak load is 1.2 times the base-case load. In addition, this paper assumes the following:

1) The load increases with a constant power factor.
2) All load increases are supplied by infinite bus.

TABLE I
The Parameters of DERs

	DERs	Bus	Capacity
IEEE 33-bus system	PV	7, 11, 12, 21, 25, 27, 33	800kVA
	PEV	7,14	100/7kW
IEEE 141-bus system	PV	5, 10, 17, 21, 27, 32, 38, 43, 49, 52, 56, 59, 64, 68, 78, 82, 89, 94, 99, 118, 124, 130, 133	800kVA
	PEV	6, 30, 55, 78, 95, 130, 141	100/7kW

A. Static Voltage Stability Analysis at Different Times

In this paper, Latin hypercube sampling [24] with a sample size of 10,000 [25] is adopted to perform probabilistic assessments of load margins at different time instants. From Fig. 7, it can be seen that MCS converges when the number of samples is about 10,000, which is consistent with the conclusion in [25]. The resulting probability distributions of load margin and the temporal trends of the probabilistic assessment indices are present in Fig. 6 and Fig. 7, respectively.

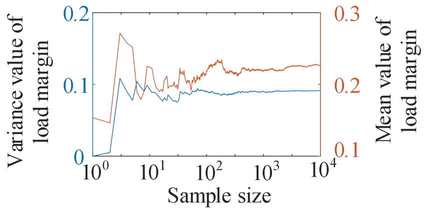

Fig. 5. Convergence curve of sample size.

As shown in Fig. 6 and Fig. 7, under the influence of multidimensional non-Gaussian random variables, the probability distribution of load margin exhibits pronounced non-normal characteristics. With increasing distributed PV, the probability density curve of load margin shifts rightward, and the expected load margin gradually increases. However, in two simulation distribution network, the dispersion of the margin distribution also widens significantly. At t=11:00, the load margin spans a range of approximately 0.1. By t=5:00, the superposition of the PEV charging uncertainty further broadens the distribution interval to approximately 0.3. At t=23:00, the PV output decreases to zero, while the EV charging demand reaches its peak. Consequently, load margin reaches its lowest value across the studied period: S are merely 0.2016 in IEEE 33-bus system and 0.1595 in IEEE 141-bus system, which is close to the predefined critical threshold for normal operation.

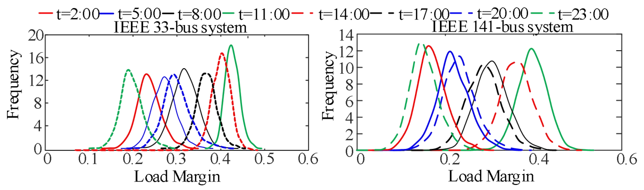

Fig. 6. Probability distribution of the static voltage stability margin at different times

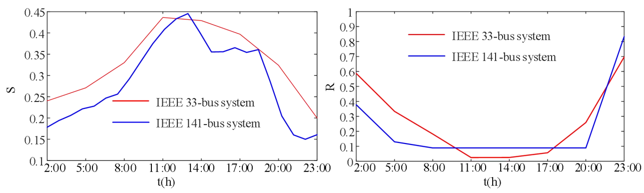

Fig. 7. Change trend of the static voltage stability probability evaluation index

B. Validation of the Improved CPF

To validate the performance of the proposed improved CPF, the following three cases are considered: Case 2.1 (base case): The P-V curve tracked by PSCAD, and the load growth rate is set at 0.001 MW/s to simulate a gradual increase in load; Case 2.2: The P-V curve tracked by the improved CPF, and the current limitation and low-voltage tripping behavior are considered; Case 2.3: The P-V curve tracked by traditional CPF, and the current limitation and low-voltage tripping behavior are not considered.

As shown in Fig. 8, when U_{PCC} drops below 0.9 p.u., the slow load growth rate results in only a minor deviation between the actual voltage and the 0.9 p.u. threshold. Consequently, the reactive power support provided by DERs is insufficient to restore the voltage above 0.9 p.u. Under the sustained influence of gradual load increase, U_{PCC} continues to decline slowly, eventually triggering the disconnection of DERs. This behavior is accurately captured by the P-V curve obtained from the PSCAD simulation in Case 2.1. The proposed improved CPF, specifically enhanced to account for this slow-load-growth characteristic, effectively tracks the P-V curve under continuously increasing load conditions. As a result, the dynamic process can be reasonably approximated using static power flow results, thereby enabling an accurate estimation of the load margin that explicitly incorporates dynamic characteristics. As the power system approaches the static voltage stability limit, the Jacobian matrix approaches singularity. Consequently, the P-V curve tracked by PSCAD reaches the voltage collapse point at a lower loading level than that tracked by the proposed CPF, yielding a reduced loading margin.

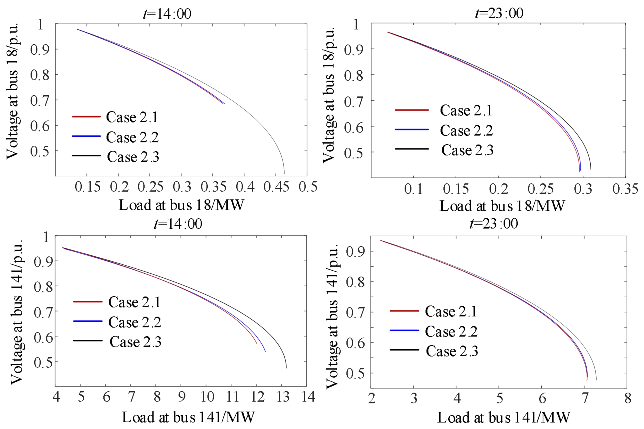

Fig. 8. The P-V curve tracked in different cases.

C. Impact of Dynamic Characteristics at Different Times

To analyze the impact of current limitations and low-voltage tripping behavior on static voltage stability at different times, the following two cases are considered:

Case 3.1: The current limitation and low-voltage tripping behavior are not considered; Case 3.2: The current limitation and low-voltage tripping behavior are considered.

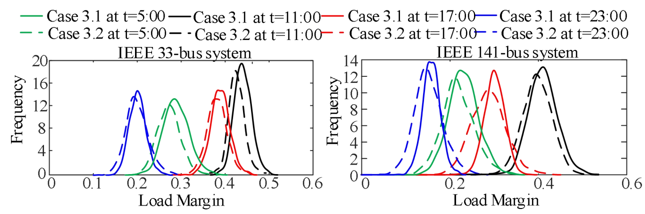

Fig. 9. The impact of current limitation and low-voltage tripping behavior.

As shown in Fig. 9, compared with current limitations, low-voltage tripping behavior has a more significant effect on system static voltage stability. However, the introduction of current limitations accelerates the rate of voltage decline during load growth, leading to earlier DER tripping, and consequently, faster voltage collapse of the system. The influence varies at different times: At t=5:00, the current limitation primarily affects the reactive power provided during the LVRT, while the low-voltage tripping behavior has a more pronounced effect. At t=11:00, the current limitation not only influences the reactive power but also impacts the active power output from the distributed PV. The

979-8-3315-8138-1

case studies demonstrate that the power characteristics of DERs significantly affect static voltage stability and cannot be overlooked.

VI. Conclusion

In this paper, a probabilistic assessment method for the load margin that accounts for dual uncertainties from both renewable generation and load demand is investigated. An improved continuation power flow algorithm that incorporates dynamic characteristics of DERs, including current limitations and low-voltage tripping behavior, is proposed and validated on the IEEE 33-bus and IEEE 141-bus distribution system. The main conclusions are as follows:

(1) The integration of distributed PVs generally enhances static voltage stability; however, the actual improvement is less pronounced than that previously reported in the literature because of the effects of current limitations and low-voltage tripping behavior.

(2) Evaluation using two complementary metrics, the expected static voltage stability margin and the static voltage stability risk index, reveals that the strong stochasticity of both generation and load significantly widens the probability distribution of stability margins and increases the likelihood of voltage instability.

(3) The improved CPF adopts a new predictor-corrector considering dynamic characteristics, so the dynamic process of low-voltage tripping behavior can be reasonably approximated using static power flow results, thereby enabling an accurate estimation of load margin that explicitly incorporates dynamic characteristics.

Future work will focus on developing coordinated control strategies that explicitly leverage DER operational characteristics to enhance static voltage stability in active distribution networks.

Acknowledgment

This work is financially supported by the National Natural Science Foundation of China, “Fundamental Theory and Methods for Form Evolution and High Efficient Safe Operation of New Power Distribution Systems” project number U23B6007.

References

[1] R. Yan, N. -A. -Masood, T. Kumar Saha, F. Bai and H. Gu, "The Anatomy of the 2016 South Australia Blackout: A Catastrophic Event in a High Renewable Network," *IEEE Trans. Power Syst*, vol. 33, no. 5, pp. 5374-5388, Sept. 2018.

[2] W. Freitas, L. C. P. Da Silva and A. Morelato, "Small-disturbance voltage stability of distribution systems with induction generators," *IEEE Trans. Power Syst.*, vol. 20, no. 3, pp. 1653-1654, Aug. 2005.

[3] J. YI, W. F. Lin, F. F. Yu. et al. "Calculation method of critical penetration of renewable energy constrained by static voltage stability," *Power Syst Tech*, vol. 44, no. 8, pp. 2906-2912, Aug 2020.

[4] L. Huang, H. Xin, Z. Wang, et al, “Transient stability analysis and control design of droop-controlled voltage source converters considering current limitation,” *IEEE Trans. Smart Grid*, vol. 10, no. 1, pp. 578–591, Jan. 2019.

[5] A. D. Paquette and D. M. Divan, "Virtual impedance current limiting for inverters in microgrids with synchronous generators," *IEEE Trans. Ind. Appl*, vol. 51, no. 2, pp. 1630-1638, March-April 2015.

[6] K. Kawabe and K. Tanaka, "Impact of Dynamic Behavior of Photovoltaic Power Generation Systems on Short-Term Voltage Stability," *IEEE Trans. Power Syst.*, vol. 30, no. 6, pp. 3416-3424, Nov. 2015.

[7] J. Yaghoobi, N. Mithulananthan and T. K. Saha, "Dynamic voltage stability of distribution system with a high penetration of rooftop PV units," *IEEE Power & Energy Society General Meeting*, Denver, CO, USA, 2015, pp. 1-5.

[8] Y. Zhao, Y. Han, Y. Liu, K. Xie, W. Li and J. Yu, "Cross-Entropy-Based Composite System Reliability Evaluation Using Subset Simulation and Minimum Computational Burden Criterion," *IEEE Trans. Power Syst.*, vol. 36, no. 6, pp. 5198-5209, Nov. 2021.

[9] A. B. Rodrigues and M. G. Da Silva, "Probabilistic Assessment of Av ailable Transfer Capability Based on Monte Carlo Method with Seque ntial Simulation," *IEEE Trans. Power Syst.*, vol. 22, no. 1, pp. 484-492, Feb. 2007.

[10] A. Schellenberg, W. Rosehart and J. A. Aguado, "Cumulant-based stochastic nonlinear programming for variance constrained voltage stability analysis of power systems," *IEEE Trans. Power Syst.*, vol. 21, no. 2, pp. 579-585, May 2006.

[11] Liu Keyan, Sheng Wanxing and Hu Lijuan, et al, "Simplified probabilistic voltage stability evaluation considering variable renewable distributed generation in distribution systems," *IET Gener. Transm Dis*, vol. 9, no. 12, pp. 1464-1473, Feb. 2015.

[12] H. Li, D. Cai, and Y. Li, "Probabilistic Assessment of Voltage Stability Margin in Presence of Wind Speed Correlation," *J Electr Eng Technol*, vol. 8, no. 4, pp. 719–728, Jul 2013.

[13] E. Haesen, C. Bastiaensen, J. Driesen and R. Belmans, "A Probabilistic Formulation of Load Margins in Power Systems with Stochastic Generation," *IEEE Trans. Power Syst*, vol. 24, no. 2, pp. 951-958, May 2009.

[14] Chengjun Xia, Xiaotian Zheng, Lin Guan, Sobia Baig, "Probability analysis of steady-state voltage stability considering correlated stochastic variables," *Int. J. Electr. Power Energy Syst*, vol.131, no. 107105, October 2021.

[15] Technical requirements for connecting photovoltaic power station to power system, Standard GB/T 19964-2024, *Standardization Administration of the P.R.C.*,2024.

[16] J. Taylor, A. Maitra, M. Alexander, D. Brooks and M. Duvall, "Evaluation of the impact of plug-in electric vehicle loading on distribution system operations," 2009 *IEEE Power & Energy Society General Meeting*, Calgary, AB, Canada, 2009, pp. 1-6.

[17] Vyas A, Santini D. Use of national surveys for estimating ‘full’ PHEV potential for oil use reduction. 2008-07-21. http://www.transportation.anl.gov/pdfs/HV/525.pdf.

[18] V. Ajjarapu and C. Christy, "The continuation power flow: a tool for steady state voltage stability analysis," *IEEE Trans. Power Syst.*, vol. 7, no. 1, pp. 416-423, Feb. 1992.

[19] Yulong Che, Xiaoru Wang and Xiaoqin Lv, et al, "Study on probability distribution of electrified railway traction loads based on kernel density estimator via diffusion," *Int. J. Electr. Power Energy Syst*, vol. 106, pp. 383-391, March 2019.

[20] Z. Qiao, Q. Guo, H. Sun, L. Jia and W. Zhao, "Static voltage stability margin considering the coupling of natural gas and power system," 2018 *IEEE Power & Energy Society General Meeting* (PESGM), Portland, OR, USA, 2018, pp. 1-5.

[21] Code on security and stability for power system, GB 38755-2019, Standardization Administration of the P.R.C., 2019.

[22] NERC, "Transmission System Planning Performance Requirements TPL-001-5," NERC.

[23] PSERC, Power System Engineering Research.Matpower4.1[EB/OL]. [2014-07-01]. http://www.pserc.cornell.edu/matpower/.

[24] H. Yu, C. Y. Chung, K and P. Wong, et al, "Probabilistic Load Flow Evaluation with Hybrid Latin Hypercube Sampling and Cholesky Decomposition," *IEEE Trans. Power Syst.*, vol. 24, no. 2, pp. 661-667, May 2009.

[25] B. Tan, J. Zhao and L. Xie, "Transferable Deep Kernel Emulator for Probabilistic Load Margin Assessment With Topology Changes, Uncertain Renewable Generations and Loads," *IEEE Trans. Power Syst.*, vol. 38, no. 6, pp. 5740-5754, Nov. 2023.